The Two Polypeptide Chains in Fibronectin Are Joined in Antiparallel Fashion: NMR Structural Characterization†

Seong Soo A. An,‡ Jesús Jiménez-Barbero,‡,§ Torben E. Petersen,‖ and Miguel Llinás*,‡

Department of Chemistry, Carnegie Mellon University, Pittsburgh, Pennsylvania 15213-3890, and Department of Molecular Biology and Plant Physiology, University of Aarhus, DK-8000 Aarhus C, Denmark

Received May 12, 1992; Revised Manuscript Received July 23, 1992

ABSTRACT: The fibronectin C-terminal interchain disulfide-linked heptapeptide dimer (Val-Asn-Cys-Pro-Ile-Glu-Cys)$_2$ has been investigated via ^{1}H NMR spectroscopy in both water and dimethyl sulfoxide (DMSO) solutions. Proton Overhauser experiments in DMSO indicate unambiguously that the two fibronectin polypeptide chains are linked head-to-tail (N-terminus to C-terminus), in an antiparallel fashion. It is found that the structure of the peptide is extended. From the ^{1}H NMR interproton distance and angle constraints, the preferred mean (time-averaged) conformations in both H_2O and DMSO were derived using distance geometry and molecular mechanics algorithms. The two conformations, although significantly dissimilar, exhibit the common feature of a structurally parallel (as opposed to chemically antiparallel) fibronectin α/β chain array.

Fibronectin is a two-chain glycoprotein of ~440 000 M_r found in blood plasma, cell surfaces, intratissue connective matrix, blood vessels, and basement membranes (McDonagh, 1985; Vartio & Vahari, 1983; Mosher, 1989; Ruoslahti, 1988). The two chains, α and β, are highly homologous and are each composed of a tandem array of repeated globular modules, generically known as type I, type II, and type III domains (Skorstengaard et al., 1986). Fibronectin is an adhesive multifunctional protein, which recognizes a wide spectrum of substrates, including fibrin, heparin, gelatin, collagen, and cell surfaces. As such, it is involved in a variety of cellular processes, including cell migration, tissue spreading, and wound healing (Vartio & Vahari, 1983; Hynes & Yamada, 1982; Hynes, 1985). Blood plasma fibronectin acts as a nonspecific opsonin that mediates the clearance of intravascular thrombi, injured platelets, and denatured proteins (Hynes & Yamada, 1982). It is also an integral component of the blood clot meshwork (Ruoslahti, 1988).

Mature human plasma fibronectin is hence dimeric. The α and β polypeptide chains are linked to each other via two disulfide bonds that involve Cys residues 2246 and 2250, within their C-terminal regions (Petersen et al., 1983). A recent study has shown that, depending on the experimental conditions, the denatured and reduced fibronectin monomers can redimerize in vitro to the correct structure (Vartio & Kuusela, 1991). Hydrodynamic experiments have indicated that fibronectin is thin, elongated, and flexible (Alexander et al., 1979). Electron microscopy (Engel et al., 1981) of fibronectin molecules reveals an extended V-shaped structure which was interpreted as indicative of parallel linkage between the α and β chains (Figure 1C). On the basis of enzymatic digestion and chromatographic analysis of the C-terminal region, Skorstengaard and co-workers (1986) have suggested that both chains are probably linked in antiparallel fashion (Figure 1A). Thus, the issue as to which is the actual dimeric form of fibronectin remains unsettled.

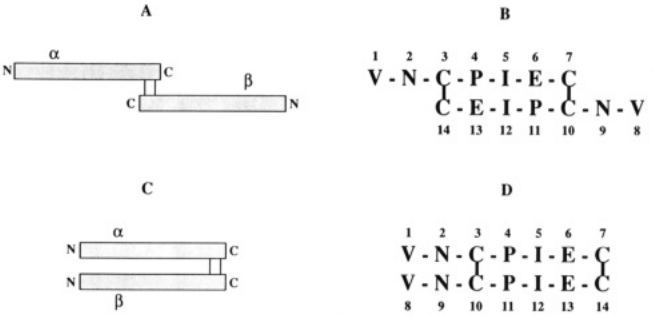

FIGURE 1: Diagram of potential fibronectin dimeric structures and primary structure of the fibronectin dimeric disulfide-linked peptide (FDLP). The antiparallel (A, B) and the parallel (C, D) disulfide chain configurations for the α and β chains are shown. Numbering of the residues from the N- to C-terminus is arbitrary; it corresponds to the Val^{2244}–Cys^{2250} segment of the fibronectin α chain paired to the Val^{2244}–Cys^{2250} segment of the β chain.

We now report a ^{1}H NMR analysis of the 14 amino acid C-terminal disulfide-linked peptide of fibronectin (FDLP,[1] Figure 1). The sequence of FDLP is conserved among all 10 fibronectin homologues sequenced to date. Two potentially occurring disulfide configurations for FDLP are possible, reflecting the two possibilities discussed above for the intact molecule: antiparallel (Figure 1B) and parallel (Figure 1D). Our study indicates that FDLP is linked in an antiparallel fashion and that the conformation of the cyclic peptide is solvent-dependent.

† This research was supported, in part, by the US Public Health Service, NIH Grant HL29409 and by the Biomembrane Centre, Danish Biotechnology Program.

‡ Carnegie Mellon University.

§ Permanent address: Instituto de Química Orgánica (CSIC), Juan de la Cierva 3, 28006 Madrid, Spain.

‖ University of Aarhus.

[1] Abbreviations: ADC, anti-distance constraints; ROESY (CAMELSPIN), rotating frame nuclear Overhauser effect spectroscopy; CGM, conjugate gradient minimization; COSY, 2D chemical shift correlated spectroscopy; DSS, 3-(trimethylsilyl)-1-propanesulfonic acid, sodium salt; DG, distance geometry; DMSO, dimethyl-d_6 sulfoxide; FDLP, fibronectin disulfide-linked peptide; FDAV, average structure of FDLP-D; FHAV, average structure of FDLP-H; FLDP-D, FDLP structures in DMSO; FDLP-H, FDLP structures in H_2O; HPLC, high-pressure liquid chromatography; NOE, nuclear Overhauser effect; NOESY, 2D nuclear Overhauser effect spectroscopy; RMSD, root-mean squares deviation; ROE, rotating frame nuclear Overhauser effect; SA, simulated annealing; TMS, tetramethylsilane; 2D, two dimensional; 1D, one dimenisonal.

0006-2960/92/0431-9927$03.00/0

MATERIAL AND METHODS

Preparation of Fibronectin Disulfide-Linking Peptide. Bovine plasma fibronectin from 80 L of blood was isolated on gelatin-Sepharose as described (Skorstengaard et al., 1982) and digested with plasmin (McDonagh et al., 1981). The fragments obtained were passed through a gelatin-Sepharose column in 50 mM ammonium bicarbonate and the nonabsorbed fragments were freeze-dried. This material was redissolved in 50 mM ammonium bicarbonate and fractionated on a Sephacryl S-200 column (4 × 75 cm) in the same buffer. Analytical digests with thermolysin were performed on small aliquots of the effluent and analyzed by HPLC. The FDLP peptide eluted at 20.3 min on a Nucleosil C-18 column (0.46 × 25 cm) developed in 0.1% trifluoroacetic acid with a gradient of acetonitrile (0–30 min; 10–40% acetonitrile). The fractions containing the C-terminal peptide were then pooled and freeze-dried. This material was digested with thermolysin (1:100 w/w) for 20 h at 37 °C in a 50 mM pyridine–acetate buffer, at pH 6.5. After lyophilization, the FDLP peptide was purified on a column of DEAE-Sepharose (1 × 20 cm) eluted with a gradient from 5 to 500 mM ammonium bicarbonate. The effluent was analyzed by HPLC as described above, and the fractions containing the FDLP peptide were pooled and freeze-dried. This material was used for the NMR studies.

NMR Spectroscopy. The concentration of FDLP was ~8 mM at pH 6.5. Solutions in H_2O contained 10% (v/v) D_2O. Deuterated chemicals, D_2O and DMSO-d_6, were obtained from Merck, Sharp and Dohme Ltd., Montréal.

NMR experiments were performed at 500 MHz using a Bruker AM-500 spectrometer, equipped with an Aspect AM-3000 computer and a 24 bit array processor. Two-dimensional (2D) experiments were processed on a Bruker X-32 station. Chemical shifts, expressed in parts per million relative to TMS (in DMSO) or DSS (in H_2O or D_2O) were measured by reference to the residual protons in Me_2SO-d_5, assumed to resonate at 2.490 ppm, or to internal dioxane (in H_2O/D_2O), resonating at 3.766 ppm. A sweep width of 5000 Hz was used for the 1D experiments yielding a digital resolution of 0.16 Hz. Scalar spin–spin (J) coupling constants were estimated from the 1D splittings. 2D ^1H NMR experiments were performed in the phase-sensitive mode using TPPI (Marion & Wüthrich, 1983). Suppression of the water signal for the experiments in H_2O and D_2O was accomplished by presaturation of the corresponding transition during the 2.5-s delay between pulses. The spectrum in H_2O was analyzed also by reference to a parallel study in D_2O. COSY experiments (Marion & Wüthrich, 1983) involved a 512 × 4 K data matrix which was zero-filled 1 K along t_1 and multiplied by a sine-bell function in each dimension prior to Fourier transformation. TOCSY experiments (Braunschweiler & Ernst, 1983; Bax & Davis, 1985a,b) were recorded via a DIPSI-2 sequence (Shaka et al., 1988). A data matrix of 384 × 4 K was obtained, zero-filled as described above, and multiplied by a 60°-shifted squared sine-bell prior to Fourier transformation. Base-plane correction was accomplished using a third-order polynomial function. 2D-ROESY/CAMELSPIN (Bothner-By et al., 1984; Bax & Davis, 1985a,b) spectra were recorded using the pulse sequence proposed by Rance (1987, 1990), the mixing time being composed of a train of 28° pulses (Kessler et al., 1987) intercalated between two 170° pulses of double amplitude (Dezheng et al., 1989) and two Z-filters. While spin-locking, the rf carrier was set 1.5 ppm high-field (in H_2O and DMSO), or 1 ppm low-field (in D_2O), relative to the center of the spectral range. Otherwise, it was centered within the spectrum. A Hahn echo was included before acquisition in order to minimize baseline distortion (Davis, 1989). The nominal strength of the spin-lock field was about 2500 Hz. A total of 384 increments of 64 scans each were accumulated using mixing times of 150, 250, and 400 ms in DMSO and 250 and 400 ms in D_2O or H_2O. Processing was identical to that described above for TOCSY experiments. Peak volumes were determined after base-plane correction using Bruker software and corrected for offset effects which depend on the effective fields affecting the spins involved (Bax, 1988). Hartmann–Hahn artifacts occurring during the 2D-ROESY experiments were discriminated against by noting the phase of the cross-peaks. NOESY experiments (Bodenhausen et al., 1984) were performed in H_2O solution at 308 and 318 K, with mixing times of 250 and 400 ms, and processed as described above for the 2D-ROESY experiments.

Structure Calculations. Cross-peak volumes from ROESY (Metzler et al., 1989) or NOESY spectra were measured. The ROE volumes were corrected for offset from the locking field. The interproton distances were estimated using the isolated spin pair approximation, by reference to the geminal proton cross-peak of Asn^2 taken to be 1.8 Å apart (Wüthrich, 1986). This is justified in view of the small size of FDLP, which ought to yield negligible spin diffusion. The DSPACE 4.0 program (Hare Research) was used to determine the 3D structures, following approaches described in the literature (Hare, 1986; Metzler et al., 1989; Summers et al., 1990). The upper and lower distance bounds were set at ±25% of the estimated distance. The prochiral atoms were assigned from NOE, ROE, and J-coupling analysis (Güntert et al., 1989).

All calculations were performed on a Silicon Graphics Personal Iris 35/4D computer. Structures were computed via a distance geometry (DG) algorithm and optimized using a molecular mechanics/energy minimization aprroach. Several hundreds of initial DG structures were generated. The initial structures were then subjected to several cycles of conjugate gradient energy minimization (CGM; Patel et al., 1987) to remove strains caused by covalent distortion. The cutoff for the nonbonded interaction distance was set to 10 Å so as to account for all possible interactions. The chiralities in these structures were corrected and subjected to a simulated annealing (SA) protocol that includes the SHAKE algorithm to enforce proper bond geometries (Nerdel et al., 1988). After the SA step, another cycle of CGM was performed. The optimized structures yielded a new set of interproton distances which were subsequently compared to those estimated from the experimental NOEs. Further refinements were carried out by interactively adjusting the interproton distance constraints, until a satisfactory agreement between the calculated structures and the NMR data was obtained. In the case where an NOE or ROE between any two protons was not observed experimentally, it was assumed, rather conservatively, that the lower distance bound between them was 3.0 Å (De Vlieg et al., 1986). These constraints were implemented as "anti-distance constraints" (ADCs) (Braunschweiler et al., 1991) in the first two cycles of structure searches. A total of 197 ADCs were enforced for the DMSO data, while 273 were used for the H_2O analysis. After implementation of ADCs, the structures were randomized by 0.4–0.7 Å per coordinate and subjected to two rounds of SA/CGM optimization. However, prior to the final restrained minimizations, all ADCs were removed.

RESULTS AND DISCUSSION

Assignment of ^1H Resonances. The spectra of FDLP showed only one set of signals, supporting a symmetric average (NMR time scale) structure for the dimeric peptide. The

Table I: ^{1}H Chemical Shifts and Spin–Spin Coupling Constants of the Fibronectin Disulfide-Linked Heptapeptide

		δ (ppm)[a]					^3J (Hz)[b]	
solvent	amino acid	NH	CH$^\alpha$	CH$^\beta$	CH$^\gamma$	CH$^\delta$	NH–H$^\alpha$	H$^\alpha$–CH$^\beta$
H_2O	Val^1		3.86	2.25	1.04 (γ, m)			6.0 ± 0.3
					1.03 (γ, m)			
	Asn^2		4.86	2.75		7.60		8.3 ± 0.5
				2.87		6.90		6.2 ± 0.5
	Cys^3	8.65	4.97	3.02 (r)			6.5 ± 0.5	10.0 ± 0.3
				3.30 (s)				3.5 ± 0.3
	Pro^4		4.54	2.44	2.10	3.98	7.5 ± 0.3	
					2.04	3.73	7.5 ± 0.3	
	Ile^5	8.12	4.13	1.95	1.51	0.93 (δ, m)	6.0 ± 0.5	6.5 ± 0.5
					1.29	0.99 (γ, m)		
	Glu^6	8.43	4.39	2.11 (s)	2.31		6.7 ● 0.4	4.5 ± 0.5
					2.01 (r)			9.0 ± 0.4
	Cys^7	7.90	4.54	2.95 (r)			8.2 ± 0.3	8.0 ● 0.5
				3.10 (s)				3.0 ± 0.3
DMSO	Val^1		3.30	2.19	0.96 (γ, m)			6.0 ± 0.4
					0.92 (γ, m)			
	Asn^2		4.75	2.66		7.28		6.6 ± 0.6
				2.27		6.68		6.6 ± 0.3
	Cys^3	8.06	4.67	2.86 (r)			7.0 ± 0.4	11.0 ± 0.5
				2.95 (s)				1.8 ± 0.3
	Pro^4		4.41	2.07	1.89	3.67		
					1.94	3.63		
	Ile^5	7.84	4.05	1.75	1.43	0.82 (δ, m)	7.0 ± 0.6	
					1.11	0.84 (γ, m)		
	Glu^6	7.54	4.41	1.86	2.2		8.0 ± 0.3	
					1.72			
	Cys^7	7.70	4.13	3.07 (r)			6.5 ± 0.5	8.5 ± 0.8
				3.21 (s)				4.8 ± 0.3

[a] ^{1}H Chemical shifts in H_2O are referred to the DSS signal using *p*-dioxane as internal standard (3.766 ppm, at 309 K, pH 6.50); in DMSO, they are referred to the TMS signal using DMSO as internal standard (2.49 ppm, 318 K). Stereospecifically assigned protons are referred to as r (pro-*R*) and s (pro-*S*). Methyl resonances are denoted by m. [b] ^3J values were estimated from the ^{1}H–^{1}H spin–spin splittings in 1D spectra.

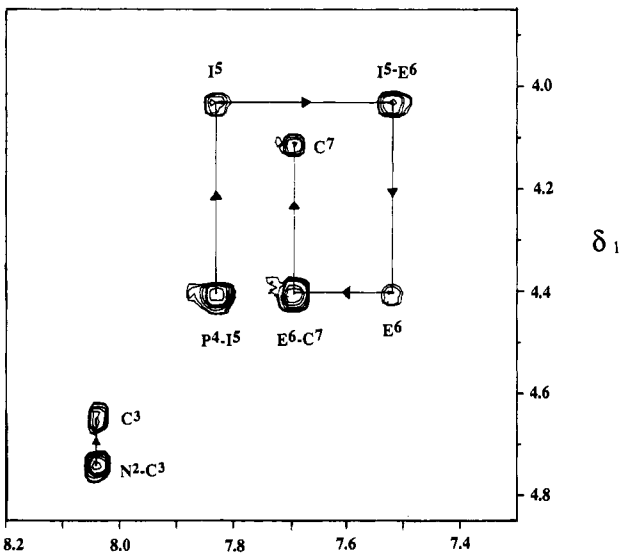

FIGURE 2: ^{1}H NMR 2D-ROESY spectrum of FDLP: H^N–H$^\alpha$ connectivities (fingerprint region). The sequential cross-peaks are indicated by arrows linking Asn^2 H$^\alpha$ to Cys^3 H$^\alpha$ and Pro^4 H$^\alpha$ to Cys^7 H$^\alpha$. The spectrum was recorded at pH 6.5, 308 K, with a mixing time of 150 ms.

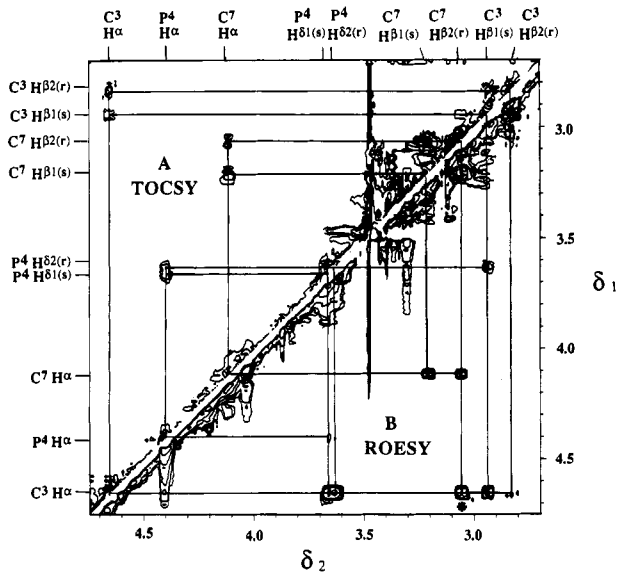

FIGURE 3: Combined ^{1}H NMR 2D spectra of FDLP. A TOCSY experiment is shown above the diagonal (A); the corresponding ROESY experiment is shown below the diagonal (B). Cross-peaks are identified by labels on the margin. The ROE between the Cys$^{3/10}$ H$^\alpha$ and the Cys$^{14/7}$ H$^{\delta 2}$ is indicated with an asterisk (*). The experiments were recorded with mixing times of 60 (TOCSY) and 150 ms (ROESY); the sample was dissolved in DMSO, at 308 K.

complete resonance assignments (Table I) were obtained from analysis of 2D COSY, TOCSY, NOESY, and ROESY spectra (Wüthrich, 1986; Ernst et al., 1987; Bax, 1989). No effort was made to detect the peptide backbone amide NH signals from the N-terminal Val$^{1/8}$ and Asn$^{2/9}$ residues. The backbone sequential connectivities were revealed by the NOESY and ROESY experiments (Figure 2). The Cys (Cys$^{3/10}$ and Cys$^{7/14}$ spin systems were unambiguously distinguished. Furthermore, strong NOEs connecting the Cys$^{3/10}$ H$^\alpha$ to the Pro$^{4/11}$ H$^{\delta 1}$ and H$^{\delta 2}$ indicated that Pro$^{4/11}$ assumes a dominant trans conformation in both H_2O and DMSO solutions (Figure 3B).[2]

1D spectra were recorded between 295 and 325 K in H_2O and between 295 and 338 K in DMSO. The amide NH

[2] Weak ROESY cross-peaks, such as the one neighboring (Pro^{4}Ile^5) the cross-peak in Figure 2, suggest that the potential presence, in equilibrium, of a *cis*-Pro^4 isomer can not be excluded.

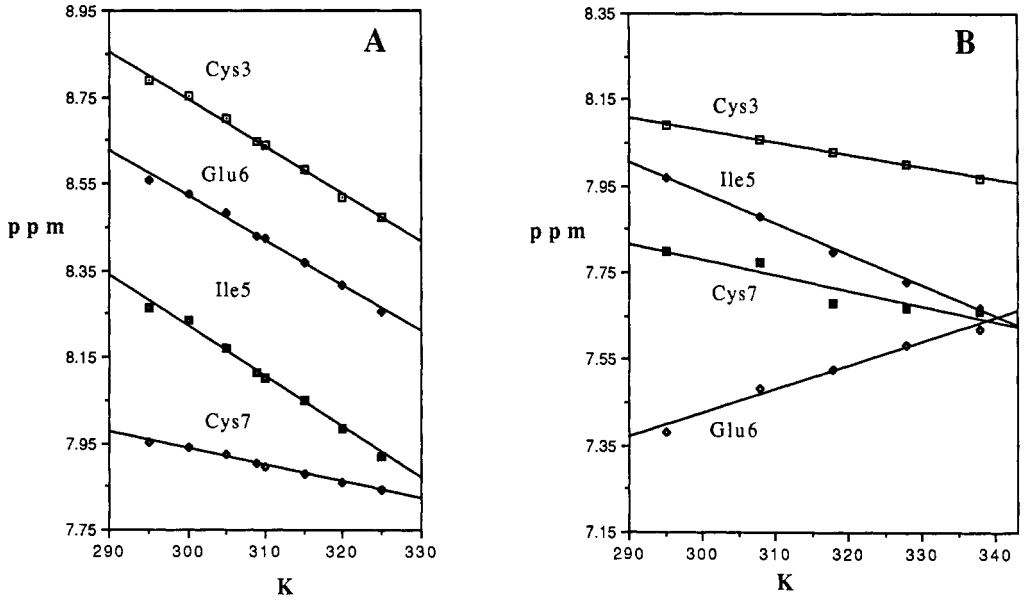

FIGURE 4: Amide chemical shift temperature profile of FDLP dissolved in H_2O (A) and in DMSO (B). The linear temperature coefficients, in (ppm/K) × 10^3, are as follows: Cys^3 (−11, −2.8), Ile^5 (−12, −7.1), Glu^6 (−10, 5.5), and Cys^7 (−3.8, −3.7), for aqueous and DMSO solutions, respectively.

chemical shift temperature profiles are plotted in Figure 4. In H_2O, the temperature profiles (Figure 4A) indicate that the amide NH hydrogens of Cys^3, Ile^5, and Glu^6 are exposed to the solvent ($\Delta\delta/\Delta T \leq -10 \times 10^{-3}$ ppm/K). In contrast, the Cys^7 amide NH group exhibits a significantly reduced temperature coefficient ($\Delta\delta/\Delta T = -3.8 \times 10^{-3}$ ppm/K), which suggests that it is partially shield and/or intramolecularly hydrogen bonded. On going to DMSO (Figure 4B), the protection of Cys^7 NH seems to be maintained ($\Delta\delta/\Delta T = -3.7 \times 10^{-3}$ ppm/K). This would be consistent with the extra rigidity imposed on the Cys^7 residue by the disulfide bridge, which would lower its dynamic exposure to the solvent. The DMSO data (Figure 4B) also indicate that the Cys^3 amide is partially protected ($\Delta\delta/\Delta T = -2.8 \times 10^{-3}$ ppm/K), consistent with the above interpretation, and suggest that, relative to the situation in H_2O, the structure in DMSO is somewhat better defined (less flexible). It is also noteworthy that the Glu^6 NH resonance exhibits a rather large, *positive* temperature coefficient in DMSO ($\Delta\delta/\Delta T = 5.5 \times 10^{-3}$ ppm/K), which strongly suggests (Llinás & Klein, 1975) that in this solvent the NH group is significantly buried within the peptide structure, with no hydrogen bonding (Figure 6). In contrast, the Ile^5 NH group seems to be exposed in both H_2O ($\Delta\delta/\Delta T = -12 \times 10^{-3}$ ppm/K) and DMSO ($\Delta\delta/\Delta T = -7.1 \times 10^{-3}$ ppm/K).

Values for vicinal *J*-couplings (Table I) were estimated from ^1H–^1H spin–spin splittings in 1D spectra. The values of $^3J_{N\alpha}$ in both H_2O and DMSO were not particularly informative as they range between 6 and 8 Hz (De Marco et al., 1978). $^3J_{\alpha\beta}$ values of $Val^{1/8}$, $Asn^{2/9}$, $Pro^{4/11}$, and $Ile^{5/12}$ in H_2O and $Val^{1/8}$ and $Asn^{2/9}$ in DMSO were also found to lie between 6 and 8 Hz. On the other hand, the spectra show one small ($^3J_{\alpha\beta} \sim 3.0$–$3.5$ Hz) and one large ($^3J_{\alpha\beta} \sim 8.5$–$10.0$ Hz) coupling constants for each $Cys^{3/10}$, $Glu^{6/13}$, and $Cys^{7/14}$ in H_2O and $Cys^{3/10}$ and $Cys^{7/14}$ in DMSO, indicating side-chain rotamers with $\chi^1 \sim 180°$ or −60°. In conjunction with the relative intensity of the NOESY and ROESY cross-peaks, the data enabled the prochiral assignments of these resonances, a feature which was enforced in the calculation of the structure.

Structure Computations. NOESY experiments were not particularly sensitive, a likely reflection of an unfavorable correlation time ($\omega\tau_c \sim 1$) at 500 MHz, resulting from the small size and structural flexibility of FDLP. Therefore, the conformational analysis was exclusively based on 2D-CAMELSPIN/ROESY spectra. A total of 69 intrachain and four interchain ROEs were identified in H_2O. Weak ROEs from $Cys^{7/14}$ to $Asn^{9/2}$ and $Val^{8/1}$ in H_2O were observed in H_2O. In parallel, we obtained 67 intrachain and four interchain ROEs in DMSO, in which solvent the crucial cross-peak connecting $Cys^{3/10}$ H^α to $Cys^{7/14}$ $H^{\beta 2}$ was detected (Figure 3B). A close distance between the two Cys residues unambiguously indicates an antiparallel interpeptide array for FDLP. In this configuration, Cys^3 from one chain is covalently linked to Cys^{14} of the other chain. This key NOE could not be unequivocally detected in H_2O as the Cys^3 H^α resonance overlaps with the residual ($^1H^2HO$) water peak. Furthermore, ROEs connecting $Cys^{7/14}$ to $Asn^{9/2}$ and to $Val^{8/1}$ were also observed in DMSO.

Distance information was derived from analysis of ROESY or NOESY data, based on the assumption that the cross-peak intensities are directly proportional to the corresponding cross-relaxation rates (spin diffusion is negligible for a peptide of this size). Totals of 146 NOE/ROE constraints for H_2O solution and 142 NOE/ROE constraints for DMSO solution were used in the structure calculation (available as Supplementary Material, Tables 2 and 3). For the $Cys^{3/10}$, $Glu^{6/13}$, and $Cys^{7/14}$ residues, the χ^1 and χ^2 torsional angles were converted into distance constraints. The floating chirality option (Weber et al., 1988) was used for the nondegenerate protons of the other residues. Methyl groups were represented by pseudoatoms (Wüthrich et al., 1983), and no hydrogen-bonding constraints were enforced in the structure calculation.

Since the NMR spectra are indicative of total magnetic equivalence between the two heptapeptide chains, *C*2 symmetry was assumed and implemented as an additional structural constraint. In order to discriminate intra- from interchain NOEs (Kessler et al., 1991), we analyzed the output structures for consistency with the experimental interproton distances. When in doubt, alternating structures were computed, and the output with the lowest number of constraint violations was selected.

The starting structures for DMSO and H_2O solutions were generated independently. From the experimental constraints,

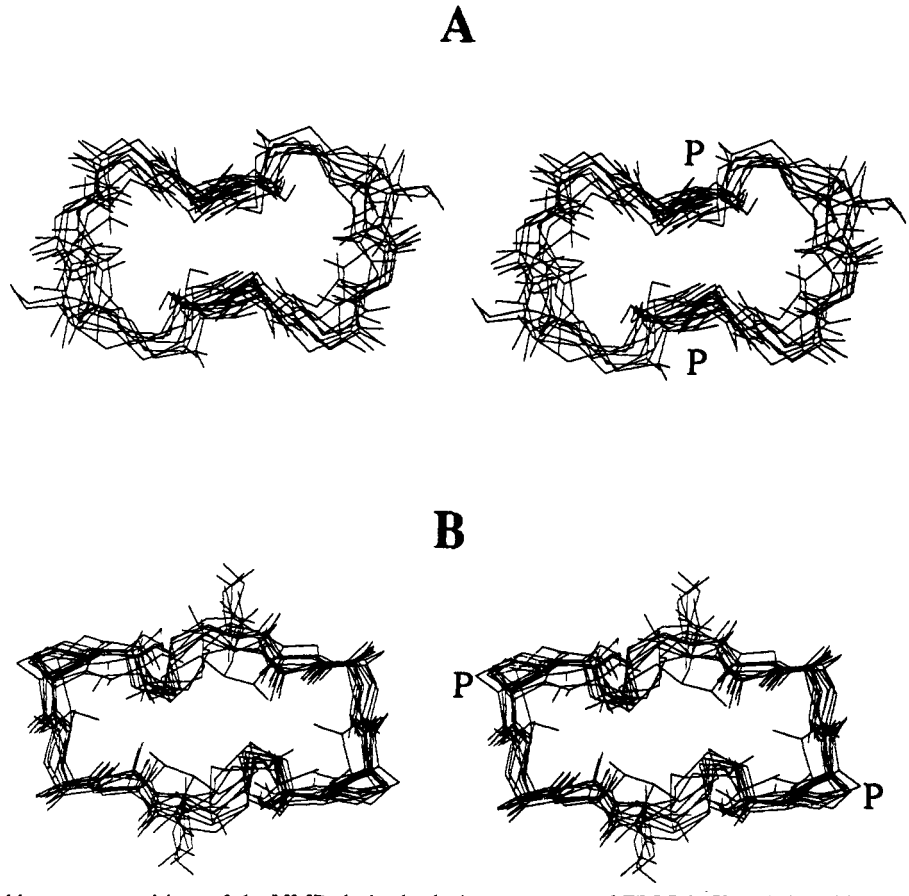

FIGURE 5: Peptide backbone superpositions of the NMR-derived solution structures of FDLP in H_2O (A) and in DMSO (B), FDLP-H and FDLP-D, respectively. P denotes the Pro residues. The N-terminal $Val^{1/8}$–$Asn^{2/9}$ dipeptide tails have been deleted for simplicity.

200 starting structures for each solvent were generated and refined as described under Material and Methods. For the simulated annealing, the explicit *C*2 symmetry was lifted allowing for motional freedom within the limits defined by the constraint bounds. The structures with no chirality violations, distance violations <0.1 Å, and proper dihedral angles were selected and compared pairwise on the basis of the backbone (N–C^{α}–C′) and cystine bridge (C^{β}–S^{γ}–S^{γ}–C^{β}) of residues 3–7 and 10–14. We selected the 10 best structures in each solvent. Approximately 15% of all the embedded structures were refined to match these criteria. [Other structures with no violations were also observed, albeit with low frequency (1–2%) and relatively removed from the average structure.] Next, ADCs were removed, and the structures were subjected to 640 steps of CGM. It is gratifying to note that the structures did not drift significantly from the starting local minimum. In what follows, we refer to these as FDLP-D (structures in DMSO) and FDLP-H (structures in H_2O) (Figure 5). The averaged structures, FHAV (Figure 6A) and FDAV (Figure 6B), from FDLP-H and FDLP-D, respectively, were calculated and subjected to a new cycle of CGM. The conformation of the N-terminal dipeptide, $Val^{1/8}$–$Asn^{2/9}$ was not clearly defined by the experimental data, suggesting major variations in their conformation, a reflection of high local flexibility. Hence, they were neglected when computing RMSDs. The average pairwise backbone RMSD between FHAV and FDLP-H structures was 0.78 ± 0.38 Å, while that between FDAV and FDLP-D structures was 0.55 ± 0.26 Å. We eventually removed all the NOE/ROE and dihedral angle constraints and applied a new cycle of CGM. These structures did not drift significantly from both FDLP-D and FDLP-H (RMSDs < 0.88 Å).

Conformations of FDLP. The superpositions of 10 FDLP-H and 10 FDLP-D are shown in Figure 5, panels A and B, respectively. The right-handed disulfide bridge conformation (Richardson, 1981) is observed for both families of structures. The dihedral angles of the $Cys^{3/10}$–$Cys^{14/7}$ disulfide bridges are 104° for FDAV and 110° for FHAV, respectively. The backbone dihedral angles indicate that FDLP-H and FDLP-D are characterized by extended chain conformations, consistent with the NOE constraints. Carbonyl oxygens are exposed along the edges of the ring rather than in the central region of the ring plane. In DMSO (Figure 6B), the Cys^7 amide NH can interact closely with carboxyl group of the side chain of Glu^6 and its own C-terminus (NH–CO ~2.4 Å). This is consistent with the low temperature coefficient for the amide in this solvent ($\Delta\delta/\Delta T = -3.7 \times 10^{-3}$, Figure 4B). In turn, the model in DMSO shows the Cys^3 amide NH to be in a relatively shielded environment as it is enclosed between the cystine bridge and the dipeptide N-terminal segments which tends to surround it in circular fashion (Figure 6B). The Glu^6 NH orients itself toward the interior of the molecule, suggesting hindered solvent accessibility. Again, this is in agreement with their reduced temperature coefficients in this solvent ($\Delta\delta/\Delta T = 5.5 \times 10^{-3}$, Figure 4B). No intramolecular hydrogen-bonding is indicated for the major conformations in either DMSO and H_2O.

CONCLUSIONS

The C-terminal region of fibronectin has been speculated to be somewhat structured (Engel et al., 1981; Mosher, 1989), consistent with our observation. The mean (time-averaged) conformation of FDLP is substantially different in H_2O than in DMSO. Thus, FDLP undergoes a conformational equi-

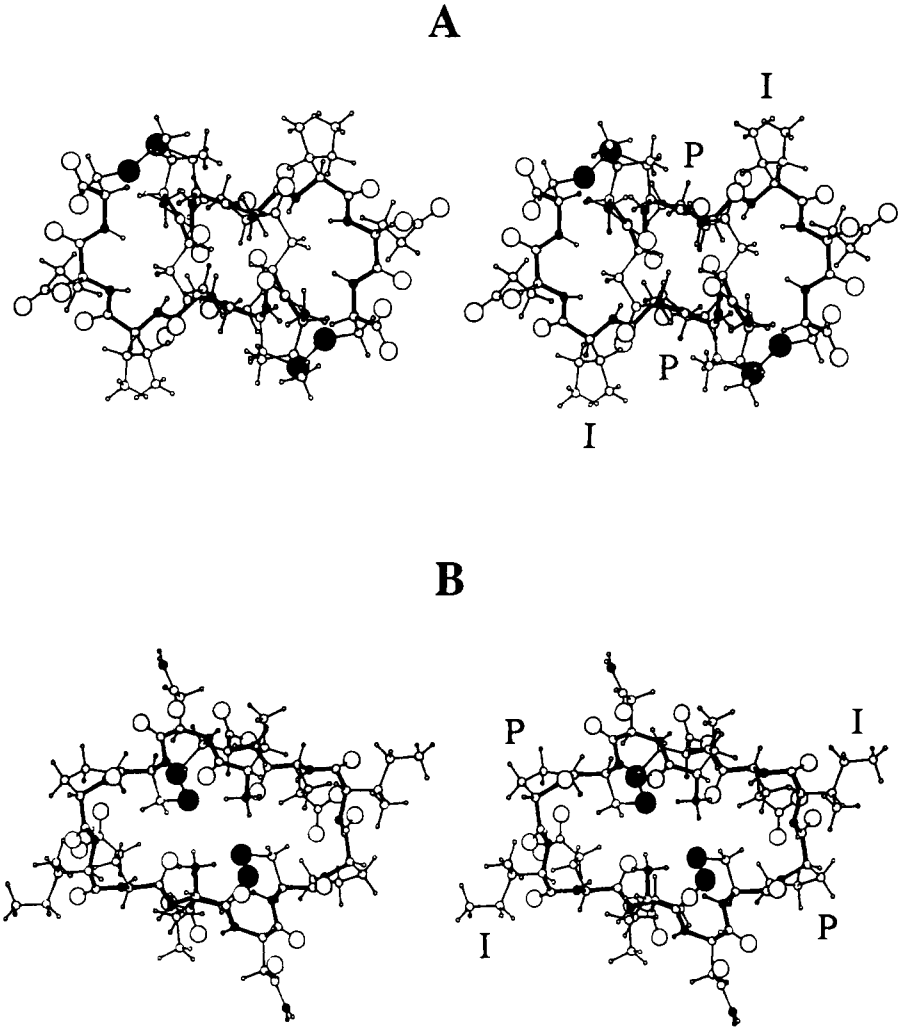

FIGURE 6: Stereoviews of the optimized average structures of FDLP in H_2O (A) and in DMSO (B), FHAV and FDAV, respectively. P and I label the Pro and Ile residues. Cystine sulfur atoms are denoted by full black circles.

librium, which is solvent dependent. Furthermore, since in each solvent FDLP yields a single ^1H NMR spectrum, the two paired fibronectin chains are linked in a unique, thermodynamically favored dimeric state. This concurs with recent in vitro dimerization studies of fibronectin (Vartio & Kuusela, 1991), suggesting a single resulting dimeric structure. The NMR evidence also indicates that the two polypeptide chains of fibronectin are linked in an antiparallel fashion (Figure 1A). Both the antiparallel array of the two chains and the structural flexibility of the joining segment would be consistent with fibronectin being an adhesive, fibrous protein that recognizes a variety of substrates while assisting cell migration without strict directional constraints. This would be in agreement with the view that the FDLP segment lacks any specific function other than that of holding fibronectin together (McDonagh, 1985).

However, although the head-to-tail antiparallel array of the α and β chains might suggest the possibility of a conformation akin to that of an extended fiber (Figure 1A), the molecular models derived for FDLP dissolved in two rather dissimilar solvents, H_2O and DMSO, independently point to a conserved structural feature that contradicts such a view, namely, that relative to each other the two chains are effectively disposed *in a parallel fashion*. Thus, the cyclic (antiparallel dimer) $-[Cys\text{-}Pro\text{-}Ile\text{-}Glu\text{-}Cys]_2$ peptide, which is primarily constrained by the two cystine bridges and by the Pro residues, acts akin to a terminal notch that holds the α and β chains together rather than like a linear junction between mutually extending chains. As depicted by the structures (Figure 6), the N-terminal Val-Asn dipeptides are disposed perpendicular relative to the average cyclopeptide backbone plane, rather than sideways, extending outward on the same plane. Although extrapolating such a feature to the intact fibronectin dimeric structure is not warranted by the data for the smaller C-terminal peptide, it is tempting to speculate that such a feature would reconcile the apparent discrepancy between the electron microscopy evidence, indicative of a V-shaped molecule (Engel et al., 1981), and the chemical (Skorstengaard et al., 1986) and NMR data, supportive of an antiparallel array.

ACKNOWLEDGMENT

J.J.-B. acknowledges the Consejería de Educación de la Comunidad de Madrid (Spain) for a fellowship. We thank Ms. Margit Jensen for expert technical assistance.

SUPPLEMENTARY MATERIAL AVAILABLE

Four tables listing backbone and cystine side-chain dihedral angles for FDAV and FHAV structures, interproton distance restraints used to generate DG structures in H_2O and DMSO, and coordinates of the average structure of fibronectin disulfide-linking heptapeptide dissolved in H_2O along with their RMSD values (13 pages). Ordering information is given on any current masthead page.

REFERENCES

Alexander, S. S., Colonna, G., & Edelbach, H. (1979) *J. Biol. Chem. 254*, 1501–1505.

Bax, A. (1988) *J. Magn. Reson. 77*, 134–147.

Bax, A. (1989) *Annu. Rev. Biochem. 58*, 223–256.

Bax, A., & Davis, D. G. (1985a) *J. Am. Chem. Soc. 107*, 2820–2822.

Bax, A., & Davis, D. G. (1985b) *J. Magn. Reson. 63*, 207–214.

Bodenhausen, G.; Kogler, H., & Ernst, R. R. (1984) *J. Magn. Reson. 58*, 370–388.

Bothner-By, A. A., Stephens, R. L., Lee, J.-M., Warren, C. D., & Jeanloz, R. W. (1984) *J. Am. Chem. Soc. 106*, 811–813.

Braunschweiler, L., & Ernst, R. R. (1983) *J. Magn. Reson. 53*, 521–528.

Braunschweiler, R., Blackledge, M., & Ernst, R. R. (1991) *J. Biomol. NMR. 1*, 3–11.

Davis, D. G. (1989) *J. Magn. Reson. 81*, 603–607.

De Marco, A., Llinás, M., & Wüthrich, K. (1978) *Biopolymers 17*, 637–650.

De Vlieg, J., Boelens, R., Scheek, R. M., Kaptein, R., & van Gunsteren, W. F. (1986) *Isr. J. Chem. 27*, 181–188.

Dezheng, Z., Toshimichi, F., & Nagayama, K. (1989) *J. Magn. Reson. 81*, 628–630.

Engel, J., Odermatt, E., Engel, A., Madrid, J. A., Furthmayr, H., Rohde, H., & Timple, R. (1981) *J. Mol. Biol. 150*, 97–120.

Ernst, R. R., Bodenhausen, G., & Wokaun, A. (1987) *Principles of Nuclear Magnetic Resonance in One and Two Dimensions*, Oxford University Press, Oxford.

Güntert, P., Braun, W., Billeter, M., & Wüthrich, K. (1989) *J. Am. Chem. Soc. 111*, 3997–4004.

Hare, D. (1986) *Biochemistry 25*, 7745–7756.

Hynes, R. O. (1985) *Annu. Rev. Cell Biol. 1*, 67–90.

Hynes, R. O., & Yamada, K. M. (1982) *J. Cell Biol. 95*, 369–377.

Kessler, H., Griesinger, C., Kerssebaum, R., Wagner, K., & Ernst, R. R. (1987) *J. Am. Chem. Soc. 109*, 607–609.

Kessler, H., Mronga, S., Müller, G., Moroder, L., & Huber, R. (1991) *Biopolymers 31*, 1189–1204.

Llinás, M., & Klein, M. (1975) *J. Am. Chem. Soc. 97*, 4731–4737.

Marion, D., & Wüthrich, K. (1983) *Biochem. Biophys. Res. Commun. 113*, 967–978.

McDonagh, J., Ed. (1985) *Plasma Fibronectin*, M. Dekker Inc., New York.

McDonagh, R. P., McDonagh, J., Petersen, T. E., Thøgersen, H. C., Skorstengaard, K., Sottrup-Jensen, L., Magnusson, S., Dell, A., & Morris, H. R. (1981) *FEBS Lett. 127*, 174–178.

Metzler, W. J., Hare, D., & Pardi, A. (1989) *Biochemistry 28*, 7045–7052.

Mosher, D. F., Ed. (1989) *Fibronectin*, Academic Press, New York.

Nerdal, W., Hare, D., & Reid, B. R. (1988) *J. Mol. Biol. 201*, 717–721.

Patel, D. J., Shapiro, D. J., & Hare, D. (1987) *Annu. Rev. Biophys. Biophys. Chem. 16*, 423–454.

Petersen, T. E., Thøgersen, H. C., Skorstengaard, K., Vibe-Pedersen, K., Sahl, P., Sottrup-Jensen, L., & Magnusson, S. (1983) *Proc. Natl. Acad. Sci. U.S.A. 80*, 137–141.

Rance, M. (1987) *J. Magn. Reson. 74*, 557–564.

Rance, M. (1990) *J. Magn. Reson. 87*, 363–372.

Richardson, J. S. (1981) *Adv. Protein Chem. 34*, 167–172.

Ruoslahti, E. (1988) *Annu. Rev. Biochem. 58*, 375–413.

Shaka, A. J., Lee, C. J., & Pines, A. (1988) *J. Magn. Reson. 77*, 274–293.

Skorstengaard, K., Thøgersen, H. C., Vibe-Pedersen, K., Petersen, T. E., & Magnusson, S. (1982) *Eur. J. Biochem. 128*, 605–623.

Skorstengaard, K., Thøgersen, H. C., Vibe-Pedersen, K., Petersen, T. E., & Magnusson, S. (1986) *Eur. J. Biochem. 161*, 441–453.

Summers, M. F., South, T. L., Kim, B., & Hare, D. (1990) *Biochemistry 29*, 329–340.

Vartio, T., & Vahari, A. (1983) *Trends Biochem. Sci. 8*, 442–444.

Vartio, T., & Kuusela, P. (1991) *Eur. J. Biochem. 202*, 597–604.

Weber, P. L., Morrison, R., & Hare, D. (1988) *J. Mol. Biol. 204*, 483–487.

Wüthrich, K. (1986) *NMR of Proteins and Nucleic Acids*, John Wiley & Sons, New York.

Wüthrich, K., Billeter, M., & Braun, W. (1983) *J. Mol. Biol. 169*, 947–961.